Journal of Alloys and Compounds 511 (2012) 74–80

Contents lists available at ScienceDirect

Journal of Alloys and Compounds

journal homepage: www.elsevier.com/locate/jallcom

Synthesis, crystal structure, spectrum properties, and electronic structure of a new barium aluminoborate, $Ba_8[(Al_6^{IV})(Al_2^{IV})(Al_2^{V})B_{12}^{III}O_{41}]_\infty$

Xuean Chen [a,*], Zhipeng Chu [a], Xinan Chang [a], Hegui Zang [a], Weiqiang Xiao [b]

[a] College of Materials Science and Engineering, Beijing University of Technology, Ping Le Yuan 100, Beijing 100124, PR China
[b] Institute of Microstructure and Property of Advanced Materials, Beijing University of Technology, Beijing 100124, PR China

ARTICLE INFO

Article history:
Received 30 May 2011
Received in revised form 4 August 2011
Accepted 5 August 2011
Available online 30 August 2011

Keywords:
$Ba_8Al_{10}B_{12}O_{41}$
Borate
Crystal structure
Band structure

ABSTRACT

A new barium aluminoborate, $Ba_8[(Al_6^{IV})(Al_2^{IV})(Al_2^{V})B_{12}^{III}O_{41}]_\infty$, has been prepared by solid state reaction method below 770 °C, with adding Bi_2O_3 as a flux. Single-crystal XRD analysis showed that it crystallizes in the triclinic space group $P\bar{1}$ with $a = 9.2437(11)$ Å, $b = 9.8100(12)$ Å, $c = 11.0830(14)$ Å, $\alpha = 76.130(10)°$, $\beta = 73.550(9)°$, $\gamma = 77.990(10)°$, $Z = 1$. The crystal structure contains Latin capital H letter shaped $Al_6O_{19}^{20-}$ groups built up from six *corner-sharing* AlO_4 tetrahedra. The $Al_6O_{19}^{20-}$ groups, AlO_4 tetrahedra, AlO_5 trigonal bipyramids, and BO_3 triangles are linked to form a two-dimensional $[(Al_6^{IV})(Al_2^{IV})(Al_2^{V})B_{12}^{III}O_{41}]^{16-}$ layer by sharing O vertices. The layers are stacked along the *c*-axis, with the interlayer void spaces and intralayer open channels occupied by Ba^{2+} cations to balance charge. The IR spectrum further confirmed the presence of BO_3 groups. UV–Vis diffuse reflectance spectrum showed a band gap of about 3.10 eV. Solid-state fluorescence spectrum exhibited a broad emission band at around 430 nm. Band structure calculations indicated that it is a direct band material with the calculated band gap (3.25 eV) close to the observed one.

1. Introduction

Borate materials have been extensively studied because they show a great variety of physical properties ranging from nonlinear optical (NLO), ferroelectric to semiconducting behaviors and in addition, a boron atom may adopt triangular or tetrahedral oxygen coordination, the BO_3 and BO_4 groups may be further linked *via* common oxygen atoms to form isolated rings and cages or polymerize into infinite chains, sheets and networks, leading to the rich structural chemistry [1,2]. The aluminium-containing borates have attracted much research interest in the past few years because $K_2Al_2B_2O_7$ (KABO) crystallizes in a noncentrosymmetric space group *P*321 and was shown to be a potential NLO material with excellent mechanical properties and a wide transparent range from 180 to 3600 nm. Using KABO crystals, it is possible to realize fourth harmonic generation at 266 nm and sum-frequency generation at 193 nm of the Nd-based lasers. These UV laser sources are widely used in medical, lithography, optical storage applications, etc. [3,4]. When two K^+ ions in KABO are replaced by one Ba^{2+} ion, $BaAl_2B_2O_7$ is obtained [5]. This compound was reported to have a noncentrosymmetric structure with space group *R*32 and the calculated second harmonic generation (SHG) coefficients are about twice as large as those of KABO [6]. Several other ternary barium aluminoborates have also been proposed including $Ba_{10}Al_2B_2O_{16}$, $Ba_5Al_4B_{12}O_{29}$, $Ba_2Al_2B_8O_{17}$, $BaAlBO_4$, $Ba_3Al_4B_4O_{15}$, $BaAl_2B_4O_{10}$, and $BaAl_3BO_7$ [7,8]. However, only the powder XRD data of these compounds have been given in the literature and their crystal structures remain as yet undetermined.

In an attempt to synthesize non-centrosymmetric compounds that are potentially applicable as NLO materials, we have successfully obtained single crystals of $Ba_8[(Al_6^{IV})(Al_2^{IV})(Al_2^{V})B_{12}^{III}O_{41}]_\infty$. Our X-ray structural analyses established that this compound ($BaO/Al_2O_3/B_2O_3 = 1.6:1:1.2$) crystallizes in a new structure-type (Pearson symbol *aP71*) and its powder XRD pattern was close to that of "$Ba_3Al_4B_4O_{15}$ ($BaO/Al_2O_3/B_2O_3 = 1.5:1:1$)" reported by Hubner [7]. Although this compound does not exhibit SHG effects, its crystal structure, IR, UV–Vis diffuse reflectance, and emission spectra as well as electronic structure calculations are presented here for the first time.

2. Experimental

2.1. Syntheses

The title compound was synthesized by employing high-temperature solid state reaction method, with adding Bi_2O_3 as a flux. All reagents were of analytical grade. For the preparation of $Ba_8[(Al_6^{IV})(Al_2^{IV})(Al_2^{V})B_{12}^{III}O_{41}]_\infty$ crystals, a powder mixture of 1.1824 g Bi_2O_3, 1.5024 g $BaCO_3$, 0.5940 g $Al(OH)_3$, 0.7844 g H_3BO_3 ($Bi_2O_3/BaCO_3/Al(OH)_3/H_3BO_3$ molar ratio = 1:3:3:5) was transferred to a 10 mL Au crucible. The sample was gradually heated to 770 °C, where it was kept for

* Corresponding author. Tel.: +86 10 62546928; fax: +86 10 67392383.
E-mail address: xueanchen@bjut.edu.cn (X. Chen).

0925-8388/$ – see front matter © 2011 Elsevier B.V. All rights reserved.
doi:10.1016/j.jallcom.2011.08.047

Table 1
Crystallographic data for $Ba_8[(Al_6^{IV})(Al_2^{IV})(Al_2^{V})B_{12}^{III}O_{41}]_\infty$.

Formula	$Ba_8Al_{10}B_{12}O_{41}$
Formula weight	2154.24
Crystal size (mm^3)	$0.20 \times 0.10 \times 0.10$
Space group	$P\bar{1}$(No.2)
a (Å)	9.2437(11)
b (Å)	9.8100(12)
c (Å)	11.0830(14)
α (°)	76.130(10)
β (°)	73.550(9)
γ (°)	77.990(10)
V (Å^3), Z	925.1(2), 1
d_{calc} (g/cm^3)	3.867
μ (mm^{-1})	8.745
$2\theta_{max}$ (°)	59.98
Unique reflection	5370
Observed [$I \geq 2((I)$]	4436
No. of variables	322
GOF on F_o^2	1.077
R1/*wR2* [$I \geq 2((I)$]	0.0334/0.0780
R1/*wR2* (all data)	0.0449/0.0801

four weeks, then cooled down to 400 °C at a rate of 0.5 °C/h, followed by cooling to room temperature at a rate of 20 °C/h. The colorless, prismatic crystals of $Ba_8[(Al_6^{IV})(Al_2^{IV})(Al_2^{V})B_{12}^{III}O_{41}]_\infty$ were observed on the surface regions of the sample contacting the wall of the Au crucible. They were separated mechanically from the reaction product for the further characterization by single-crystal and powder XRD measurements. The crystals were also checked by energy-dispersive X-ray analyses in a scanning electron microscope, which confirmed the presence of heavy elements of barium and aluminium with an approximate atomic ratio of 4:5. Although Bi was not incorporated into the final structure, Bi_2O_3 was found to act as a flux for the crystal growth. In the synthesis of the title compound, a stoichiometric mixture of $BaCO_3$, $Al(OH)_3$, and H_3BO_3 did not melt when heated until 850 °C. The addition of Bi_2O_3 in a molar ratio of $Bi_2O_3/BaCO_3/Al(OH)_3/H_3BO_3 = 1:3:3:5$ resulted in a lower melting point of about 780 °C. When this sample was kept at 770 °C for four weeks, it was partially melt, which is favorable for the formation of $Ba_8[(Al_6^{IV})(Al_2^{IV})(Al_2^{V})B_{12}^{III}O_{41}]_\infty$ crystals. The polycrystalline sample was obtained by grinding the crystals and powder XRD analyses confirmed the phase purity. Moreover, this compound is relatively stable in air and water, but soluble in hot diluted HNO_3 solution.

2.2. Structure determination

Single-crystal X-ray intensity data were collected at room temperature (290 K) on an automated Rigaku AFC7R four-circle diffractometer using monochromatized Mo Kα radiation ($\lambda = 0.71073$ Å). Cell dimensions were first obtained from a least-squares refinement with 25 automatically-centered reflections. Subsequently, searching in ICSD (Inorganic Crystal Structure Database) indicates that the cell dimensions are different from those of the known borate crystalline phases; therefore, the intensity data are further collected. The data were corrected for Lorentz and polarization effects, and for absorption by empirical method based on ψ-scan data. The crystal structure was solved by a direct method and refined in SHELX-97 system [9] by full-matrix least-squares methods on F_o^2. After introduction of anisotropic displacement parameters for all atoms, the refinement of 322 parameters with 4436 observed reflections [$I \geq 2((I)$] resulted in the residuals of *R1*/*wR2* = 0.0334/0.0780. The final difference electron density map was featureless, with the residual electron densities less than 3.02 e Å^{-3} at positions which are very close to heavy atomic sites. Details of crystal parameters, data collection and structure refinements are given in Table 1 and the atomic coordinates and the equivalent isotropic displacement parameters are summarized in Table 2.

2.3. Spectral measurements

Infrared spectra were recorded from 4000 to 400 cm^{-1} on a Perkin Elmer 1730 FT-IR spectrometer from KBr pellets. Optical diffuse reflectance spectra were measured at room temperature with a Shimadzu UV-3101PC double-beam, double-monochromator spectrophotometer. Data were collected in the wavelength range 200–1100 nm. $BaSO_4$ powder was used as a standard (100% reflectance). A similar procedure as previously described [10,11] was used to collect and convert the data using the Kubelka–Munk function $F(R) = (1-R)^2/2R$, where R is the reflectance. The minima in the second-derivative curves of the Kubelka–Munk function are taken as the position of the absorption bands. The emission spectrum was measured on an F-7000 time-resolved fluorescence spectrometer using a Xe lamp at room temperature.

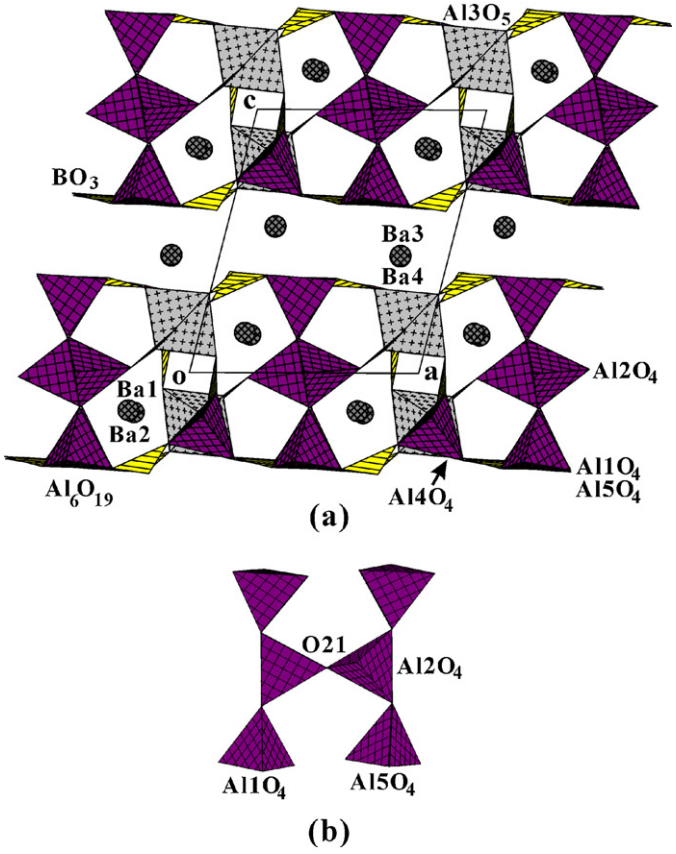

Fig. 1. The crystal structure of $Ba_8[(Al_6^{IV})(Al_2^{IV})(Al_2^{V})B_{12}^{III}O_{41}]_\infty$ projected along the *b*-axis (a) as well as the Latin capital H letter shaped $Al_6O_{19}^{20-}$ group (b). Ba atoms: circles with grid lines; AlO_4 groups: tetrahedra with grid lines; AlO_5 groups: trigonal bipyramids with crosses; BO_3 groups: triangles with parallel lines.

2.4. Electronic structure calculations

Energy band, density of states (DOS), and optical property calculations were performed using a first principle plane-wave pseudopotential technique based on density functional theory (DFT) with CASTEP code [12] distributed inside a computational commercial pack [13]. The ion–electron interaction was modeled by the norm-conserving pseudopotential [14]. Local density approximation (LDA) of CA-PZ scheme was employed to evaluate exchange-correlation energy [15,16]. Pseudoatomic calculations were performed for Ba $5s^2\ 5p^6\ 6s^2$, Al $3s^2\ 3p^1$, B $2s^2\ 2p^1$, and O $2s^2\ 2p^4$. A kinetic energy cut-off of 330.0 eV was used for plane wave expansions in reciprocal space. The calculating parameters and convergent criterions were set by the default values of CASTEP code [13]. The calculations of linear optical properties described in terms of the complex dielectric function $\varepsilon = \varepsilon_1 + i\varepsilon_2$ were also made in this work. The imaginary part of the dielectric function, $\varepsilon_2(\omega)$, can be described as detailing the real transitions between occupied and unoccupied electronic states. The real and imaginary parts are linked by a Kramers–Kronig transform [17].

3. Results and discussion

3.1. Description of the structure

$Ba_8[(Al_6^{IV})(Al_2^{IV})(Al_2^{V})B_{12}^{III}O_{41}]_\infty$ has a complicated porous layered structure [Fig. 1(a)]. The primary building blocks in this structure are AlO_4 tetrahedra, AlO_5 trigonal bipyramids, and BO_3 triangles. Six AlO_4 tetrahedra form a Latin capital H letter shaped $Al_6O_{19}^{20-}$ group, which has an inversion-center at its group center (the O21 atom) and acts as a secondary building block [Fig. 1(b)]. The $Al_6O_{19}^{20-}$ groups, AlO_4 tetrahedra, and AlO_5 trigonal bipyramids are bridged by BO_3 triangles through sharing O atoms to form a two-dimensional (2D) infinite $[(Al_6^{IV})(Al_2^{IV})(Al_2^{V})B_{12}^{III}O_{41}]^{16-}$ layer extending in the (0 0 1) plane. The *inversion-center-related*

Table 2
Atomic coordinates and equivalent isotropic displacement parameters (Å^2) for $Ba_8[(Al_6^{IV})(Al_2^{IV})(Al_2^{V})B_{12}^{III}O_{41}]_\infty$.

Atoms	*X*	*Y*	*Z*	U_{eq}
Ba1	0.22351(4)	1.05143(4)	0.14415(3)	0.01226(8)
Ba2	0.19689(4)	0.57237(3)	0.15211(3)	0.00936(7)
Ba3	0.21069(3)	0.42929(3)	0.55368(3)	0.00761(7)
Ba4	0.78927(3)	0.05742(3)	0.44297(3)	0.00813(7)
Al1	0.41668(17)	0.71082(17)	0.29634(16)	0.0067(3)
Al2	0.54714(19)	0.66103(19)	0.00717(17)	0.0112(3)
Al3	0.89502(18)	0.86524(17)	0.18750(16)	0.0076(3)
Al4	0.87116(19)	0.36259(17)	0.20354(16)	0.0082(3)
Al5	1.42043(17)	0.20800(17)	0.29355(16)	0.0065(3)
B1	0.0957(6)	0.7843(6)	0.3542(6)	0.0075(10)
B2	0.5675(6)	0.9249(6)	0.3351(5)	0.0066(10)
B3	0.5606(7)	0.4240(6)	0.3374(6)	0.0085(11)
B4	0.8231(7)	0.6506(7)	0.0902(6)	0.0121(12)
B5	0.8798(7)	0.1576(6)	0.0603(6)	0.0105(11)
B6	1.0977(7)	0.2827(6)	0.3450(6)	0.0086(11)
O1	0.0768(5)	0.9132(4)	0.3805(4)	0.0126(8)
O2	0.2249(4)	0.6838(4)	0.3715(4)	0.0093(7)
O3	−0.0035(4)	0.7458(4)	0.3005(4)	0.0087(7)
O4	0.5345(4)	1.0615(4)	0.3593(4)	0.0113(8)
O5	0.7125(4)	0.8545(4)	0.3219(4)	0.0109(8)
O6	0.4460(4)	0.8648(4)	0.3343(4)	0.0135(8)
O7	0.5373(4)	0.5619(4)	0.3531(4)	0.0118(8)
O8	0.7051(4)	0.3473(4)	0.3301(4)	0.0106(8)
O9	0.4406(4)	0.3645(4)	0.3352(4)	0.0116(8)
O10	0.8267(5)	0.7906(4)	0.0876(4)	0.0120(8)
O11	0.8945(4)	0.5432(4)	0.1677(4)	0.0103(7)
O12	0.7401(5)	0.6172(5)	0.0184(4)	0.0186(9)
O13	0.8590(5)	0.2969(4)	0.0759(4)	0.0140(8)
O14	0.9019(5)	0.1350(4)	−0.0615(4)	0.0135(8)
O15	0.8814(4)	0.0530(4)	0.1678(4)	0.0100(7)
O16	1.0148(4)	0.2499(4)	0.2708(4)	0.0124(8)
O17	1.0631(4)	0.4069(4)	0.3843(4)	0.0112(8)
O18	1.2268(4)	0.1850(4)	0.3653(4)	0.0096(7)
O19	0.4263(4)	0.7322(4)	0.1347(4)	0.0143(8)
O20	0.5604(5)	0.7840(5)	−0.1340(4)	0.0163(9)
O21	1/2	1/2	0	0.0156(12)

Note: U_{eq} is defined as one third of the trace of the orthogonalized **U** tensor.

$[(Al_6^{IV})(Al_2^{IV})(Al_2^{V})B_{12}^{III}O_{41}]^{16-}$ layers are stacked along the crystallographically *c*-axis and one half of Ba^{2+} cations (Ba3 and Ba4) are located between the layers to balance charge and also to hold the layers together *via* electrostatic interactions. The aluminium borate anionic layer also affords three kinds of one-dimensional (1D) open channels running parallel to the [0 1 0] direction, of which the largest channels are created from the edges of two AlO_4 tetrahedra, one AlO_5 trigonal bipyramid, and three BO_3 triangles and occupied by the rest of Ba^{2+}cations (Ba1 and Ba2). The other tunnels with a pentagonal or square window are too small to be filled by Ba^{2+}cations.

As seen from Fig. 2 and Table 2, the asymmetric unit of $Ba_8[(Al_6^{IV})(Al_2^{IV})(Al_2^{V})B_{12}^{III}O_{41}]_\infty$ contains 36 independent atoms, i.e., 4Ba, 5Al, 6B, and 21O, of which one O atom (O21) lies on an *inversion-center* and the other atoms occupy crystallographic general positions. Four distinct barium atoms are divided into two sets: Ba1 is surrounded by ten O atoms forming an irregular polyhedral coordination geometry and the other Ba atoms are each coordinated to nine O atoms in an approximately tri-capped trigonal prismatic configuration. The Ba–O distances of 2.755(4)–3.351(5) Å (average 3.001 Å, Table 3) for Ba1 and 2.684(4)–3.115(4) Å (average 2.820–2.850 Å) for Ba2–Ba4 are very reasonable when compared with the values 2.90 Å and 2.85 Å computed from crystal radii for a 10- and 9-coordinated Ba^{2+} ion, respectively [18]. These distances are also close to those observed in $BaCu(B_2O_5)$ [2.702(6)–3.000(5) Å, average 2.88 Å, CN = 10] [19] and $BaNa(BO_3)$ [2.759(7)–3.012(6) Å, average 2.845 Å, CN = 9] [20]. Bond valence sum (BVS) calculations using Brown's formula [21] produced BVS values of 1.74–2.17 for the Ba atoms, in good agreement with the expected formal valence.

Of the five unique aluminium atoms, one (Al3) adopts trigonal bipyramidal oxygen coordination geometry and the others have typical tetrahedral coordination configuration. The Al–O bonds in the trigonal bipyramid range from 1.772(4) to 1.998(4) Å and the O–Al–O angles are divided into three sets:86.19(18)–94.00(18)°, 118.38(19)–120.9(2)°, and 173.75(19)°, respectively, while in the tetrahedra the Al–O distances are slightly shorter, at 1.710(4)–1.778(5) Å and the O–Al–O angles merged into one set: 102.2(2)–115.8(2)° (see Table 4). These geometric parameters are comparable to those observed in the structures of $BaAl_2B_2O_7$ [5] and $SrO(Al_2O_3)_6$ [22], where AlO_4 and AlO_5 groups were also observed, respectively. The calculated BVS values are 2.70–2.86 for the Al atoms, supporting the choice of four- or five-fold coordination to describe the Al environment. Note that tetrahedral and octahedral coordination geometries are preferred by Al atoms, as found in a number of compounds, e.g., $BaAl_2B_2O_7$ [5], $K_3AlB_8O_{15}$ [23], $TmAl_3(BO_3)_4$ [24], and $BiCd_3(AlO)_3(BO_3)_4$ [25]; AlO_5 trigonal bipyramids are rather rare, but have been previously reported in the structure of $SrO(Al_2O_3)_6$ [22], while the unusual Latin capital H letter shaped $Al_6O_{19}^{20-}$ group composed of six corner-sharing AlO_4 tetrahedra, to the best of our knowledge, is present here for the first time.

The boron atoms reside in six distinct triangular sites. The B–O bond lengths vary from 1.330(7) to 1.409(6) Å with average values of 1.372–1.379 Å, which are consistent with those reported in other orthoborates, e.g., $AlBO_3$ [1.380(1) Å] [26], $FeBO_3$ [1.379(2) Å] [27], $InBO_3$ [1.380(1) Å] [28], $LuBO_3$ [1.370(1) Å] [29], and $ScBO_3$ [1.375(1) Å] [30]. The O–B–O bond angles cover the range between 116.5(5) and 125.3(5)° with average values of 119.9–120.0°, indicating that the triangular coordination around B atoms is almost

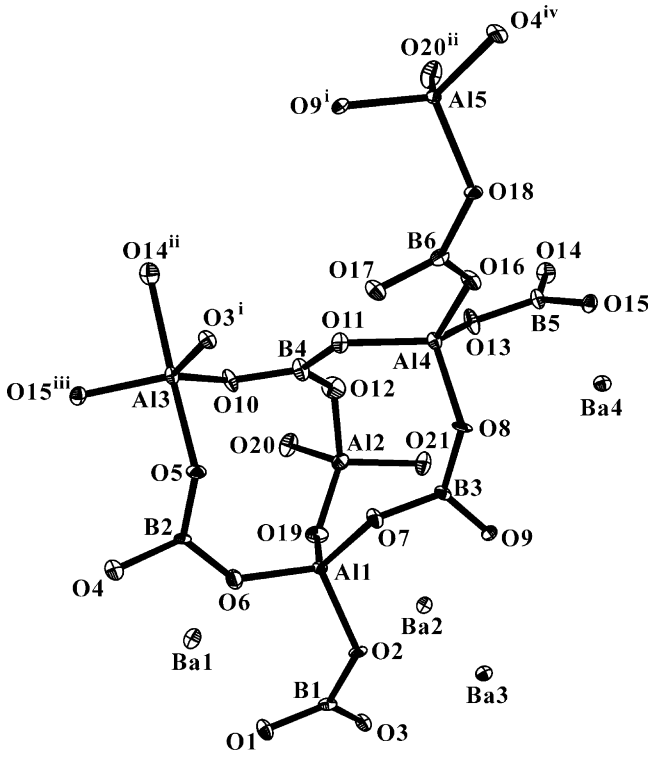

Fig. 2. ORTEP view of the asymmetric unit of $Ba_8[(Al_6^{IV})(Al_2^{IV})(Al_2^{V})B_{12}^{III}O_{41}]_\infty$ to show the atomic labeling scheme. Displacement ellipsoids are all reasonable and drawn at the 50% probability level. Symmetry codes: (i) $(1+x, y, z)$; (ii) $(2-x, 1-y, -z)$; (iii) $(x, 1+y, z)$; (iv) $(1+x, -1+y; z)$.

planar. BVS values for B atoms are also reasonable, lying in the range 2.95–3.00. In this structure, 21 unique oxygen atoms can be classified into two groups depending on their cationic bonding: O1–O18 atoms are connected to B and Ba atoms or to B, Al, and Ba atoms; while O19–O21 are bonded to Al and Ba atoms only and no B atoms observed in their coordination sphere. Thus the compound is attributed to a oxoborate.

As mentioned in Introduction, the solid equilibrium relations in the system $BaO–Al_2O_3–B_2O_3$ have been determined by Hubner *via* solid state reaction method [7]. At least six ternary compounds have been found, while only $BaAl_2B_2O_7$ has been recently structurally characterized [5]. It contains $Al_2O_7^{8-}$ groups formed by two corner-sharing AlO_4 tetrahedra. The $Al_2O_7^{8-}$ groups are bridged by BO_3 triangles through sharing O atoms to form 2D $[B_2Al_2O_7]^{2-}$ layers that are stacked rhombohedrally along the *c*-axis, with the interlayer void spaces hosting Ba^{2+} cations. The crystal structure of $BaAl_2B_2O_7$ is quite different from that of $Ba_8[(Al_6^{IV})(Al_2^{IV})(Al_2^{V})B_{12}^{III}O_{41}]_\infty$ where the layered structure is composed of corner-sharing Latin capital H letter shaped $Al_6O_{19}^{20-}$ groups, AlO_4 tetrahedra, AlO_5 trigonal bipyramids, and BO_3 triangles.

3.2. Spectrum properties

Concerning IR spectra of borates it is reported [31] that the frequencies of normal vibrations of BO_3 groups lie in the ranges $\nu_s \sim 850–960\ cm^{-1}$, $\gamma \sim 650–800\ cm^{-1}$, $\nu_{as} \sim 1100–1450\ cm^{-1}$, and $\delta \sim 500–600\ cm^{-1}$. In order to further confirm the coordination surroundings of B atoms, the infrared spectrum of the title compound was measured and shown in Fig. 3, where the bands at around $1297.3\ cm^{-1}$ may be assigned as the BO_3 antisymmetric stretching vibrations (ν_{as}); the bands near $721.6\ cm^{-1}$ caused by the out-of-plane bending vibrations (γ); and those at about $490.5\ cm^{-1}$ due to

Table 3
Selected bond lengths (Å) for $Ba_8[(Al_6^{IV})(Al_2^{IV})(Al_2^{V})B_{12}^{III}O_{41}]_\infty$.

Ba1–O1	2.755(4)	Al2–O20	1.723(4)
Ba1–O10	2.772(4)	Al2–O19	1.729(4)
Ba1–O16	2.774(4)	Al2–O21	1.7487(18)
Ba1–O20	2.782(4)	Al2–O12	1.778(5)
Ba1–O14	2.796(4)	Mean	1.745
Ba1–O18	3.054(4)	Al3–O10	1.772(4)
Ba1–O15	3.095(4)	Al3–O15	1.784(4)
Ba1–O19	3.307(4)	Al3–O3	1.823(4)
Ba1–O6	3.326(4)	Al3–O5	1.911(4)
Ba1–O12	3.351(5)	Al3–O14	1.998(4)
Mean	3.001	Mean	1.858
Ba2–O13	2.685(4)	Al4–O13	1.728(4)
Ba2–O3	2.708(4)	Al4–O16	1.760(4)
Ba2–O17	2.796(4)	Al4–O11	1.766(4)
Ba2–O11	2.821(4)	Al4–O8	1.767(4)
Ba2–O12	2.825(4)	Mean	1.755
Ba2–O19	2.829(4)	Al5–O20	1.710(4)
Ba2–O14	2.852(4)	Al5–O4	1.735(4)
Ba2–O21	2.8753(5)	Al5–O9	1.764(4)
Ba2–O2	2.987(4)	Al5–O18	1.778(4)
Mean	2.820	Mean	1.747
Ba3–O17	2.684(4)	B1–O1	1.330(7)
Ba3–O17	2.704(4)	B1–O3	1.379(7)
Ba3–O3	2.741(4)	B1–O2	1.409(6)
Ba3–O2	2.810(4)	Mean	1.373
Ba3–O7	2.827(4)	B2–O5	1.359(6)
Ba3–O5	2.837(4)	B2–O6	1.376(7)
Ba3–O9	2.837(4)	B2–O4	1.384(7)
Ba3–O11	3.024(4)	Mean	1.373
Ba3–O8	3.115(4)	B3–O9	1.364(7)
Mean	2.842	B3–O7	1.371(7)
Ba4–O1	2.689(4)	B3–O8	1.381(6)
Ba4–O1	2.722(4)	Mean	1.372
Ba4–O4	2.755(4)	B4–O11	1.371(7)
Ba4–O18	2.782(4)	B4–O10	1.374(7)
Ba4–O8	2.860(4)	B4–O12	1.380(7)
Ba4–O6	2.929(4)	Mean	1.375
Ba4–O15	2.934(4)	B5–O14	1.371(7)
Ba4–O5	2.945(4)	B5–O15	1.375(7)
Ba4–O16	3.035(4)	B5–O13	1.385(7)
Mean	2.850	Mean	1.377
Al1–O19	1.731(4)	B6–O17	1.338(7)
Al1–O7	1.747(4)	B6–O16	1.397(7)
Al1–O6	1.752(4)	B6–O18	1.402(7)
Al1–O2	1.778(4)	Mean	1.379
Mean	1.752		

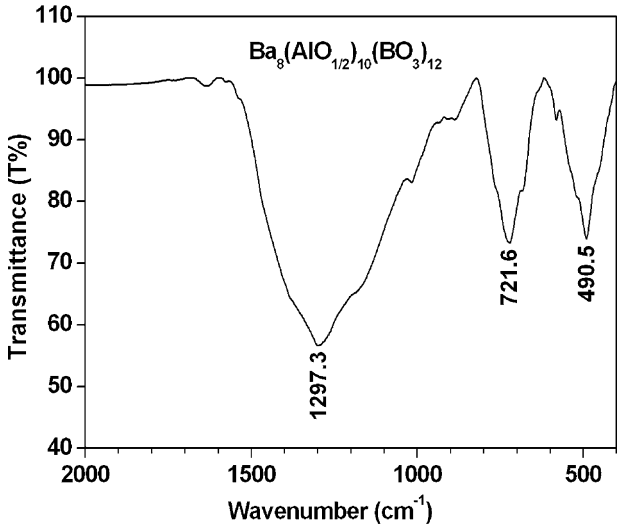

Fig. 3. Infrared spectrum of $Ba_8[(Al_6^{IV})(Al_2^{IV})(Al_2^{V})B_{12}^{III}O_{41}]_\infty$.

Table 4
Selected bond angles (°) for $Ba_8[(Al_6^{IV})(Al_2^{IV})(Al_2^{V})B_{12}^{III}O_{41}]_\infty$.

O19–Al1–O7	113.4(2)	O20–Al5–O4	112.1(2)
O19–Al1–O6	111.8(2)	O20–Al5–O9	115.8(2)
O7–Al1–O6	111.3(2)	O4–Al5–O9	111.2(2)
O19–Al1–O2	103.4(2)	O20–Al5–O18	104.0(2)
O7–Al1–O2	108.2(2)	O4–Al5–O18	107.8(2)
O6–Al1–O2	108.2(2)	O9–Al5–O18	105.11(19)
Mean	109.38	Mean	109.34
O20–Al2–O19	111.2(2)	O1–B1–O3	122.0(5)
O20–Al2–O21	113.99(17)	O1–B1–O2	121.2(5)
O19–Al2–O21	111.81(17)	O3–B1–O2	116.6(5)
O20–Al2–O12	102.2(2)	Mean	119.93
O19–Al2–O12	113.1(2)	O5–B2–O6	123.6(5)
O21–Al2–O12	103.96(17)	O5–B2–O4	119.8(5)
Mean	109.38	O6–B2–O4	116.5(5)
O10–Al3–O15	120.9(2)	Mean	119.97
O10–Al3–O3	118.38(19)	O9–B3–O7	119.7(5)
O15–Al3–O3	120.4(2)	O9–B3–O8	122.0(5)
O10–Al3–O5	93.5(2)	O7–B3–O8	118.3(5)
O15–Al3–O5	94.00(18)	Mean	120.0
O3–Al3–O5	87.62(18)	O11–B4–O10	121.2(5)
O10–Al3–O14	90.26(19)	O11–B4–O12	119.2(5)
O15–Al3–O14	88.36(18)	O10–B4–O12	119.5(5)
O3–Al3–O14	86.19(18)	Mean	119.97
O5–Al3–O14	173.75(19)	O14–B5–O15	125.3(5)
Mean	119.89, 89.99, 173.75	O14–B5–O13	117.5(5)
O13–Al4–O16	108.0(2)	O15–B5–O13	117.2(5)
O13–Al4–O11	115.0(2)	Mean	120.0
O16–Al4–O11	112.9(2)	O17–B6–O16	121.3(5)
O13–Al4–O8	111.1(2)	O17–B6–O18	121.9(5)
O16–Al4–O8	103.2(2)	O16–B6–O18	116.5(5)
O11–Al4–O8	106.0(2)	Mean	119.90
Mean	109.37		

the in-plane bending modes (δ). The IR spectrum confirms the existence of only trigonally coordinated boron atoms, consistent with the results obtained from the crystallographic study.

The optical diffuse reflectance spectrum is shown in Fig. 4. It is observed that there are no absorption bands above 400 nm, implying that the material is transparent under the visible light, while the strong absorption peaks appear at around 257 (4.82 eV) and 309 nm (4.01 eV). The absorption edge of UV–Vis diffuse reflectance spectrum is at around 400 nm, from which the optical band gap is estimated to be roughly 3.10 eV. In addition, the emission spectrum excited by an ultraviolet light of 280 nm is shown in Fig. 5, in which there exists one emission region from *ca.* 390 to 470 nm with the emitted peak localized at about 430 nm (2.88 eV). Since the emission energy of 2.88 eV is less than the optical absorption edge

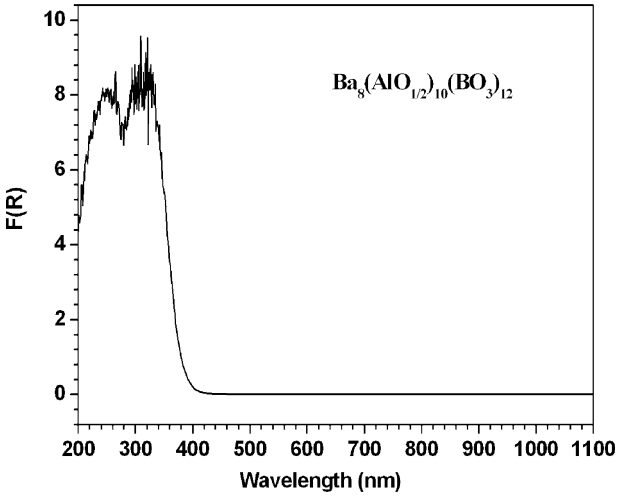

Fig. 4. Optical absorption spectrum of $Ba_8[(Al_6^{IV})(Al_2^{IV})(Al_2^{V})B_{12}^{III}O_{41}]_\infty$.

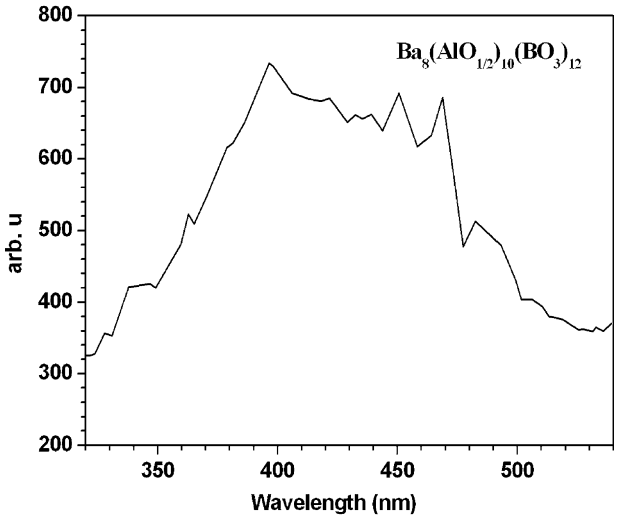

Fig. 5. Emission spectrum of $Ba_8[(Al_6^{IV})(Al_2^{IV})(Al_2^{V})B_{12}^{III}O_{41}]_\infty$.

of 3.10 eV, we can deduce that the emitted fluorescence probably originates from the defects or excitons.

3.3. Band structures, densities of states, and optical properties

The calculated band structure of $Ba_8[(Al_6^{IV})(Al_2^{IV})(Al_2^{V})B_{12}^{III}O_{41}]_\infty$ along high-symmetry points of the first Brillouin zone is shown in Fig. 6. It can be seen that the top of valence bands is almost flat, whereas the bottom of conduction bands displays some dispersion. Both the valence band maximum (VBM) and the conduction band minimum (CBM) are located at the G point, permitting the description of $Ba_8[(Al_6^{IV})(Al_2^{IV})(Al_2^{V})B_{12}^{III}O_{41}]_\infty$ as a direct band material. The calculated direct energy gap is about 3.25 eV, which is consistent with the experimental value of 3.10 eV obtained from the diffuse reflectance spectrum.

Fig. 7 gives the total density of states (DOS) and partial DOS (PDOS) projected onto the constitutional atomic orbitals of $Ba_8[(Al_6^{IV})(Al_2^{IV})(Al_2^{V})B_{12}^{III}O_{41}]_\infty$. It is found that the band structure can be divided into five principal groups separated by gaps. The lowest group with energy located at around −24.5 eV is basically of Ba 5s character. The second group ranging from −20.0 to −15.6 eV mostly originates from O 2s states, with small admixtures of B 2s/2p

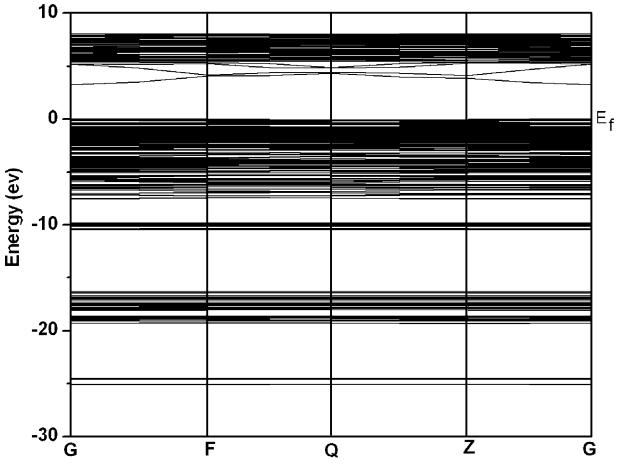

Fig. 6. The calculated band structure of $Ba_8[(Al_6^{IV})(Al_2^{IV})(Al_2^{V})B_{12}^{III}O_{41}]_\infty$, where the Fermi level (E_F) is set at 0 eV and the labeled k-points are present as $G(0, 0, 0)$, $F(0, 1/2, 0)$, $Q(0, 1/2, 1/2)$, and $Z(0, 0, 1/2)$.

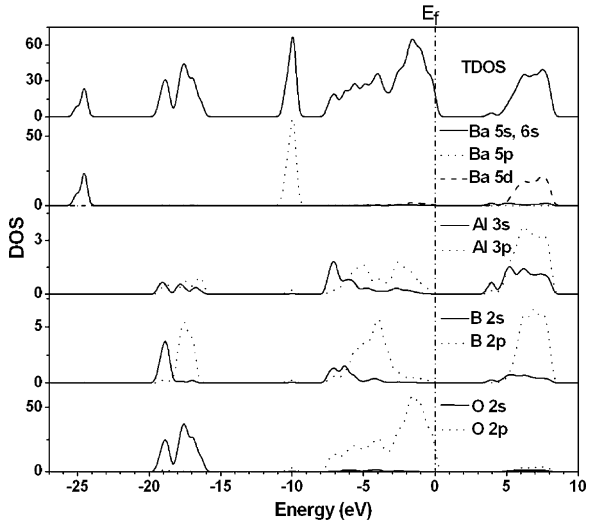

Fig. 7. Total and partial densities of states of $Ba_8[(Al_6^{IV})(Al_2^{IV})(Al_2^{V})B_{12}^{III}O_{41}]_\infty$.

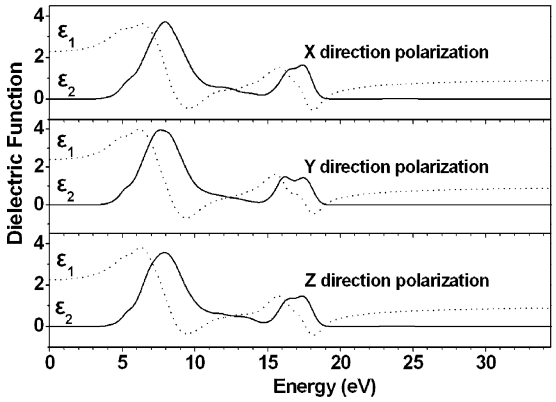

Fig. 8. Calculated real and imaginary parts of dielectric functions in different polarization directions for $Ba_8[(Al_6^{IV})(Al_2^{IV})(Al_2^{V})B_{12}^{III}O_{41}]_\infty$.

and Al 3s/3p states. The third group lying near −10.0 eV is derived from Ba 5p orbitals, with small contributions of O 2p component. The group from −8.2 eV up to Fermi energy (E_F) is mainly of O 2p character, with small admixtures of B 2s/2p and Al 3s/3p states. The group from the CBM up to 8.8 eV is dominated by the Ba 5d, B 2p, and Al 3s/3p states, mixing with small amounts of O 2p states. The electronic structure of the upper valence band arises primarily from the O 2p and B 2p states. We note that most of the O 2p character is concentrated in the upper valence band, with only negligible amounts in the conduction band and the CBM is controlled by Ba 6s states.

From the PDOS, we note a strong hybridization between B 2s/2p and O 2p and between Al 3s/3p and O 2p states in the energy region from −8.2 eV to E_F, implying that the substantial covalence interactions exist between B and O and between Al and O atoms. This is also confirmed by Mulliken bond order analysis, which is a convenient way to quantify the strength of bonding between a pair of atoms. A bond order value of zero corresponds to an ideal ionic bond, while larger values indicate a more covalent nature of the bond. The calculated bond orders of B–O, Al–O, and Ba–O bonds in a unit cell are 0.74–0.94e, 0.31–0.54e, and −0.02–0.09e, respectively, depending on the distances [1.330(7)–1.409(6), 1.710(4)–1.998(4), 2.684(4)–3.351(5) Å, respectively]. This means that the B–O bonds have stronger covalent character than the Al–O bonds as it is well known, while the Ba–O bonds are basically ionic interactions.

To evaluate and assign the observed absorption spectra, we examined the linear optical response properties of the $Ba_8[(Al_6^{IV})(Al_2^{IV})(Al_2^{V})B_{12}^{III}O_{41}]_\infty$ crystal. The calculated real (ε_1) and imaginary (ε_2) parts of dielectric functions in different polarization directions without the DFT scissor operator approximation are displayed in Fig. 8, where the spectral broadening is taken to be 0.3 eV. It can be seen from the $\varepsilon_2(\omega)$ curves that there are two absorption peaks at the lower energy region: the shoulder peak at about 5.25 eV and the strong absorption peak at about 7.95 eV in the x polarization direction (which corresponds to those at about 7.64 and 7.90 eV in the *y* and *z* polarization direction, respectively). The peaks in $\varepsilon_2(\omega)$ can correspond to electronic transitions with the same energy between the occupied and unoccupied bands. Therefore, the shoulder peak (the first absorption peak) which can be compared with the observed absorption peak at around 4.01 eV (309 nm) of the experimental spectrum (Fig. 4), is assigned as the electronic transitions from the occupied O 2p states to the mixed states of unoccupied Ba 5d, B 2p, and Al 3s/3p orbitals according to the above DOS and PDOS analyses. In addition, the calculated transparent cut-off edge of about 376 nm (3.3 eV) can be obtained from Fig. 8, which corresponds to the observed one localized at about 400 nm (3.1 eV). This absorption edge is due to the electronic transitions from the O 2p to Ba 6s states.

From the spectral dependences of imaginary parts of the dielectric function $\varepsilon_2(\omega)$ the real parts $\varepsilon_1(\omega)$ can be calculated using Kramers–Kronig relations [17]. The static dielectric constant $\varepsilon(0)$ is given by the low energy limit of $\varepsilon_1(\omega)$ [$\varepsilon(0) \approx \varepsilon_1(0)$ at low frequency]. The calculated value of $\varepsilon(0)$ is about 2.286, 2.386 and 2.253 along the *x*, *y* and *z* directions, indicating a strong anisotropy of the dielectric function. The refractive index is an important optical parameter in optical transmitted materials. It is a measure of how faster light travels in a medium and the lower the refractive index, the faster the speed of light. The knowledge of both real and imaginary parts of the frequency dependent dielectric function allows us to calculate the dispersion curves of refractive index using the relation of $n^2(\omega) = \varepsilon(\omega) = \varepsilon_1(\omega) + i\varepsilon_2(\omega)$. Based on the $n(\omega)$ curves, the refractive indexes of n_x, n_y and n_z were found to be 1.522, 1.556 and 1.510 at the wavelength of 1064 nm, respectively. Although the refractive indices of $Ba_8[(Al_6^{IV})(Al_2^{IV})(Al_2^{V})B_{12}^{III}O_{41}]_\infty$ have not been measured, our calculated results are reasonable when compared with the experimental values of $BaAl_2B_2O_7$ ($n_o = 1.570$, $n_e = 1.517$, where n_o is the index of refraction for an electric field perpendicular to the *c*-axis and n_e is the index of refraction for an electric field oriented along the *c*-axis) [32].

4. Conclusions

A novel ternary borate with the composition $Ba_8[(Al_6^{IV})(Al_2^{IV})(Al_2^{V})B_{12}^{III}O_{41}]_\infty$ has been synthesized and characterized. It has a layered structure consisting of Latin capital H letter shaped $Al_6O_{19}^{20-}$ groups, AlO_4 tetrahedra, and AlO_5 trigonal bipyramids bridged by BO_3 triangles, with the interlayer spaces and intralayer channels hosting the Ba^{2+} cations. The IR spectrum confirms the existence of only trigonally coordinated boron atoms, consistent with the results obtained from the crystallographic study. The optical properties have been investigated in terms of diffuse reflectance and fluorescent spectra, which reveal the presence of an optical gap of 3.10 eV and a broad emission band at around 430 nm upon photoexcitation at 280 nm. Band structure calculations with CASTEP code show that this compound has a direct energy gap of 3.25 eV, which is comparable with our measured value. Analyses of total and partial densities of states indicate that the top of the valence band is dominated by the O 2p states, while the bottom of the conduction band is controlled by Ba 6s states. The observed absorption peak at around 309 nm in the diffuse reflectance spectrum can be assigned as the electronic

transitions from the O 2p to the mixed states of unoccupied Ba 5d, B 2p, and Al 3s/3p orbitals and the absorption edge is due to the electronic transitions from the O 2p to Ba 6s states. In addition, dielectric constants and refractive indexes have also been calculated and the refractive indexes derived from dielectric constant are close to the observed values of $BaAl_2B_2O_7$.

Acknowledgment

This work was supported by the National Natural Science Foundation of China (Grant No. 20871012).

References

[1] P. Becker, Adv. Mater. 10 (1998) 979.
[2] J.D. Grice, P.C. Burns, F.C. Hawthorne, Can. Miner. 37 (1999) 731.
[3] C. Zhang, J. Wang, X. Hu, H. Jiang, Y. Liu, C. Chen, J. Cryst. Growth 235 (2002) 1.
[4] C. Liu, L. Liu, X. Zhang, L. Wang, G. Wang, C. Chen, J. Cryst. Growth 318 (2011) 618.
[5] N. Ye, W.R. Zeng, B.-C. Wu, X.-Y. Huang, C.-T. Chen, Z. Krist, New Cryst. Struct. 213 (1998) 452.
[6] C. Chen, Z. Lin, Z. Wang, Appl. Phys. B 80 (2005) 1.
[7] K.-H. Hubner, Neues Jahrb. Mineral. Abh. 112 (1970) 150.
[8] R. Jagannathan, R.P. Rao, T.R.N. Kutty, Mater. Res. Bull. 27 (1992) 459.
[9] G.M. Sheldrick, SHELX-97: Program for Structure Refinement, University of Goettingen, Germany, 1997.
[10] J. Li, Z. Chen, X.-X. Wang, D.M. Proserpio, J Alloys Compd. 262–263 (1997) 28.
[11] W.M.W. Wendlandt, H.G. Hecht, Reflectance Spectroscopy, Interscience: A Division of John Wiley & Sons, New York, 1966.
[12] M.C. Payne, M.P. Teter, D.C. Allan, T.A. Arias, J.D. Joannopoulos, Rev. Mod. Phys. 64 (1992) 1045.
[13] Materials Studio, Version 4.1, Accelrys Inc., San Diego, 2006.
[14] N.-J. Troullier, L. Martins, Phys. Rev. B 43 (1991) 1993.
[15] D.M. Ceperley, B.J. Alder, Phys. Rev. Lett. 45 (1980) 566.
[16] J.P. Perdew, A. Zunger, Phys. Rev. B 23 (1981) 5048.
[17] J.R. Macdonald, M.K. Brachman, Rev. Mod. Phys. 28 (1956) 383.
[18] R.D. Shannon, Acta Crystallogr. A 32 (1976) 751.
[19] R.W. Smith, D.A. Keszler, J. Solid State Chem. 129 (1997) 184.
[20] J.-M. Tu, D.A. Keszler, Acta Crystallogr. C 51 (1995) 1962.
[21] I.D. Brown, D. Altermatt, Acta Crystallogr. B 41 (1985) 244.
[22] J.-G. Park, A.N. Cormack, J. Solid State Chem. 121 (1996) 278.
[23] Y. Tanaka, J. Fukunaga, M. Setoguchi, T. Higashi, M. Ihara, J. Ceram. Soc. Jpn. 90 (1982) 458.
[24] G. Jia, C. Tu, J. Li, Z. You, Z. Zhu, B. Wu, Inorg. Chem. 45 (2006) 9326.
[25] X. Chen, H. Yin, X. Chang, H. Zang, W. Xiao, J. Solid State Chem. 183 (2010) 2910.
[26] A. Vegas, Acta Crystallogr. B33 (1977) 3607.
[27] J.R. Cox, D.A. Keszler, Acta Crystallogr. C 50 (1994) 1857.
[28] R. Diehl, Solid State Commun. 17 (1975) 743.
[29] D.A. Keszler, H. Sun, Acta Crystallogr. C44 (1988) 1505.
[30] S.C. Abrahams, J.L. Bernstein, E.T. Keve, J. Appl. Crystallogr. 4 (1971) 284.
[31] S. Filatov, Y. Shepelev, R. Bubnova, N. Sennova, A.V. Egorysheva, Y.F. Kargin, J. Solid State Chem. 177 (2004) 515.
[32] K. Yamada, Japan Kokai Tokyo Koho, Japanese Patent No. 09.61. 864 (1994).